Proceedings of ICFDP9:
Ninth International Congress of Fluid Dynamics & Propulsion
December 18-21, 2008, Alexandria, Egypt

ICFDP9-EG-215

NUMERICAL STUDY ON MULTIPHASE FLUID DYNAMICS AND TRANSPORT PROCESSES OF SUPERCAVITATING FLOWS

Guoyu Wang
Beijing Institute of Technology, China
Email: wangguoyu@bit.edu.cn

Xiangbin Li
Beijing Institute of Technology, China

Bo Zhang
Beijing Institute of Technology, China

Zhiyi Yu
Beijing Institute of Technology, China

ABSTRACT

To better understand the multiphase fluid dynamics and associated transport processes of cavitating flows at the cavitation number of 0.74 and 0.54, a computational investigation of flows around a hydrofoil is conducted. The computational model is based on a modified RNG k-ε model as turbulence closure, along with a vapor-liquid mass transfer model for treating the cavitation process. The computational results are compared with experimental ones. Overall, favorable agreement between the numerical and experimental results is observed. It is shown that the cavitation structure depends on the interaction of the water-vapor mixture and the vapor among the whole cavitation stage, the interface between the vapor and the two-phase mixture exhibits substantial unsteadiness. And, the adverse motion of the interface relates to pressure and velocity fluctuations inside the cavity. In particular, the velocity in the vapor region is lower than that in the two-phase region.

KEYWORDS:

Supercavitating flows; Multiphase dynamics; Numerical method;.

INTRODUCTION

In cavitating flows, there are large density variations, substantial pressure variations and noticeable mass transfer associated with phase changes. Depending on the cavitation number, four distinct regimes can be identified: as the cavitation number decreases, inception cavitation, sheet cavitation, cloud cavitation, and supercavitation appears [1, 2]. Furthermore, by decreasing the cavitation number, while the cavitating structure changes from discreet bubbles to contiguous multiphase domains, the cavitation generation mechanism varies from localized, instantaneous pressure drop found in inception cavitation [3], to sustained, time dependent cavities observed in cloud and sheet cavitation [4-7]. With a sufficiently low cavitation number, supercavitation occurs when the size of cavity covers the entire underwater object. Compared with other types of cavitation, in this regime, there is often a more distinct interface between the bulk liquid flow and the cavitating region. In recent years, super cavitation research has attracted growing interests due to its potential for vehicle maneuvering and drag reduction [8]. The pressure inside a supercavitation cavity is often considered to be uniform and equal to the saturation vapor pressure [9]. Based on these considerations, simplified analytical approaches have been proposed. For example, a free stream method based on the potential flow theory has been developed to predict the cavitation dynamics [10-12]. However, the potential flow analysis method does not account for the viscous and turbulent effects and is insufficient as a predictive framework for detailed analysis.

In the last decade or two, both steady state and unsteady Navier-Stokes equations-based techniques have been developed to simulate cavitation characteristics, including pressure, velocity, and phase change characteristics. Alternative computational modeling approaches have been proposed. These studies can be classified into two categories, namely, interface tracking methods [13] and homogeneous equilibrium flow models. Here, we concentrate on the homogeneous modeling approach. Reviews of this approach can be found in the references [1, 14]. Based on the homogeneous equilibrium flow theory, the mixture concept can be introduced, and mass and momentum equations along with turbulence and cavitation models can be established for the entire flow field. Specifically, two approaches have been utilized to model the cavitation

dynamics. The first one is the arbitrary barotropic equation model, which suggests that the relationship between density and pressure is $\rho = f(p)$, and the second one is the transport equation-based model (TEM). Barotropic equations were proposed by Delannoy and Kueny [15]. They assumed that density is a continuous function of pressure where both pure phases were incompressible, and the phase change could be fitted by a sine curve. Arbitrary barotropic equation models (density is only a function of pressure) can't capture baroclinic vorticity production because the baroclinic term of the vorticity transport equation yields zero by definition [15, 16]. Consistent with the experimental study [16], Senocak and Shyy have demonstrated computationally that the baroclinic vorticity generation is important in the closure region [17, 18]. In the TEM, a transport equation for either mass or volume fraction, with appropriate source terms to regulate the mass transfer between vapor and liquid phases, is adopted. An advantage of this model comes from the convective character of the equation, which allows modeling of the impact of inertial forces on cavities like elongation, detachment and drift of cavity bubbles, especially in complex 3-D interface situations [1]. Different modeling concepts embodying qualitatively similar source terms with alternate numerical techniques have been proposed by various researchers [19-21]. Numerically, Singhal et al. [19, 23], and Wu et al. [24] utilized pressure-based algorithms, while Kunz et al. [20] employed the artificial compressibility method. For flows with large property variations and high Reynolds number, the convection treatments and the boundary treatment are of importance as well. Some of the issues regarding the convection treatment can be found in Shyy [25, 26]. In addition, Vaidyanathan et al. [27] performed a sensitivity analysis on a transport equation-based cavitation model to optimize the coefficients of its source terms.

As for the turbulence model, different closures have been utilized to treat unsteady cavitating flows [24, 28, 29]. Since the high eddy viscosity in the standard k-ε model dampens the unsteady characteristics dramatically [24], alternative approaches have been adopted by modifying the eddy viscosity [30-32]. It seems that especially for unsteady flow computations, satisfactory results more critically depend on the turbulence model.

The present study focuses on the multiphase fluid dynamics related to cavitating flows at the cavitation number of 0.74 and 0.54, with cavity essentially covering the entire hydrofoil. The aspects investigated include time dependency of cavity sizes, characterization of the phase boundaries, and the pressure and velocity fields. A computational study has been conducted. The computational model is based on the Rayleigh-Plasset equation along with a modified RNG k-ε turbulence model, and a water-vapor mass transfer model, as detailed below.

1. COMPUTATIONAL APPROACH

1.1 Governing equations

The Favre averaged form of the mass conservation equation and Navier-Stokes equation for the momentum conservation are written in Cartesian co-ordinates:

$$\frac{\partial \rho}{\partial t} + \nabla \cdot (\rho \vec{u}) = 0 \tag{1}$$

$$\frac{\partial}{\partial t}(\rho \vec{u}) + \nabla \cdot (\rho \vec{u}\vec{u}) = -\nabla P + \nabla \cdot [(\mu + \mu_t)\nabla \vec{u}] + \frac{1}{3}\nabla[(\mu + \mu_t)\nabla \cdot \vec{u}] \tag{2}$$

$$\text{here,} \quad \rho = \rho_v \alpha_v + \rho_l (1 - \alpha_v) \tag{3}$$

1.2. Turbulence model

The RNG k-ε model proposed by Yakhot et al. [31] is as follows:

$$\frac{\partial(\rho k)}{\partial t} + \nabla \bullet (\rho U_k) = \nabla \bullet \left[\left(\mu + \frac{\mu_t}{\sigma_{kRNG}} \right) \nabla k \right] + p_k - \rho\varepsilon \tag{4}$$

$$\frac{\partial(\rho\varepsilon)}{\partial t} + \nabla \bullet (\rho U_\varepsilon) = \nabla \bullet \left[\left(\mu + \frac{\mu_t}{\sigma_{\varepsilon RNG}} \right) \nabla \varepsilon \right] + \frac{\varepsilon}{k}(C_{\varepsilon 1 RNG} p_k - C_{\varepsilon 2 RNG} \rho\varepsilon) \tag{5}$$

Where, the turbulent viscosity is defined as:

$$\mu_t = f(\rho) C_{\mu RNG} k^2 / \varepsilon \tag{6}$$

It was observed that the RNG k-ε model resulted in shorter cavity lengths compared to the experiments [28]. Accordingly, a modified RNG k-ε turbulence closure model, proposed by Coutier-Delgosha et al. [28], is adopted in this study. Here, the major difference is the definition of the function $f(\rho)$. Compared to $f(\rho) = \rho$ in the original model, it was defined as:

$$f(\rho) = \rho_v + (1 - \alpha_v)^n (\rho_l - \rho_v) \qquad n > 1 \tag{7}$$

where the effect of vapor phase was added.

1.3. Cavitation model

The cavitation process is governed by the thermodynamics and the kinetics of the phase change dynamics occurring in the system. Equation 8 gives the conservation equation of vapor volume fraction. Here, the source terms $\dot{m}^+$ and $\dot{m}^-$, represent evaporation and condensation of the phases [33], respectively.

$$\frac{\partial \rho_v \alpha_v}{\partial t} + \nabla \cdot (\rho_v \alpha_v \vec{u}) = \nabla \cdot (\Gamma \nabla \rho_v \alpha_v / \rho) - \dot{m}^- + \dot{m}^+ \tag{8}$$

$$\dot{m}^+ = F_e \frac{3\alpha_{nuc}(1 - \alpha_v)\rho_v}{R_B} \sqrt{\frac{2}{3}\frac{|P_v - P|}{\rho_l}} \tag{9}$$

$$\dot{m}^- = F_c \frac{3\alpha_v \rho_v}{R_B} \sqrt{\frac{2}{3}\frac{|P_v - P|}{\rho_l}} \quad (10)$$

Noting that Eqs. (9) and (10) are different from the original model proposed by Kubota et al. [33]. Since the evaporation rate is much higher than the condensation one- condensation usually occurs slowly and vaporization occurs quickly, different coefficients are imposed.

Further, several studies have shown significant effect of turbulence on cavitating flows. Specifically, the incipient cavitation number increases with the turbulence intensity of the flow [34, 35]. It seems that the local turbulent pressure fluctuation should be incorporated into the definition of the vapor pressure, so that the phase change responds to both thermodynamic and fluid dynamic conditions. In this study, we follow the model proposed by Singhal et al. [19]:

$$P_{turb} = 0.39\rho k \quad (11)$$

$$P_v = (P_{sat} + P_{turb}/2) \quad (12)$$

This approach has been found to be simple and yield more favorable outcome (Singhal [23]).

1.4. Grid, boundary and initial conditions

The two-dimensional computational domain is chosen to correctly follow the geometry of the experimental test section. An orthogonal mesh with 62,720 cells is generated. Alternative meshe systems, with 41,540 and 85,580 cells, respectively, were also chosen to evaluate the grid sensitivity of the computation. Fig. 1 gives the grid distribution, finer mesh are located around the hydrofoil and the cavitating region as the experiments indicated, to obtain more accurate cavitating results. The nondimensional distance to solid walls y+ is given between 20 and 50, which can satisfy the requirement of wall functions.

Fig. 2 shows the calculated pressure coefficients for all three meshes under steady condition. Fig. 2a indicates the whole pressure distribution, and Fig. 2b gives the zoom picture in partial position (corresponding to the circle position in Fig. 2a). It can be found that two results, computed with 62720 and 85580 cells, are similar basically. Considering the computational economy, 62720 cells are seclected as shown in Fig. 1.

The numerical simulation conditions are adopted according to the experimental processes [36]. In this study, the inflow streamwise velocity, volume fractions and turbulence quantities are specified at the inlet boundary, and the cross-sectional-averaged static pressure is imposed as the reference pressure at the outlet. A no-slip boundary condition is used at both the upper and lower walls.

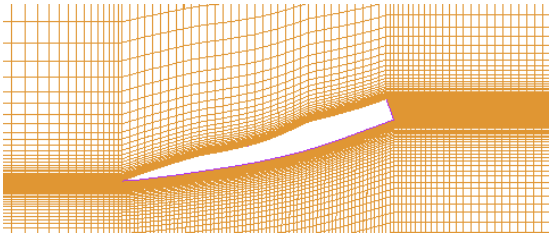

Fig. 1 Grid distribution around the hydrofoil

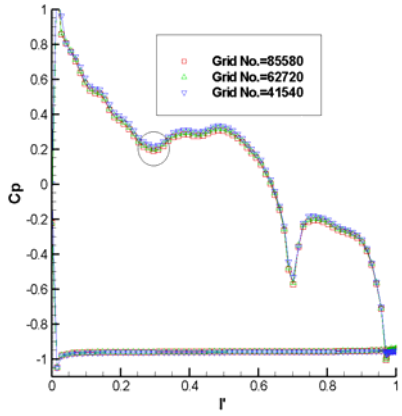

(a) Whole picture

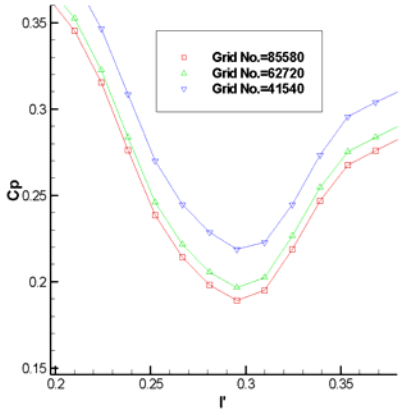

(b) Close-up picture of the circle area in (a)

Fig.2 Distribution of pressure coefficient （σ= 0.77，α=15°）

2. RESULTS AND DISCUSSIONS

In this study, the reference velocity U is fixed at 10m/s, the Reynolds number Re and the cavitation number are defined:

$$Re = Uc/\upsilon \quad (13)$$

$$\sigma=2(P\infty-Pv)/(\rho_l U^2) \quad (14)$$

The supercavitating flows around the foil have been studied numerically at 15°of attack angle. Two cavitation numbers, 0.74 and 0.54 are adopted to get different flowing structures.

To deeply grasp the motioning mechanism of the two-phase interface, the instantaneous pressure and velocity distributions are obtained at special position as shown in Figure 3. Here, three horizontal sections such as L1, L2 and L3 are captured. Taking the leading point of the foil's suction surface as the coordinate origin, L1, L2 and L3 go through the leading, middle and trailing point of the suction surface respectively.

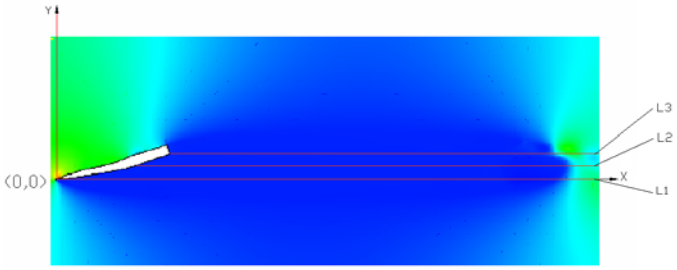

Fig. 3 Schematic of special section locations

As the cavitation number is reduced to 0.74, at 15° of attack angle, supercavitation is attained. The CFD simulation results compared with flow visualizations [36] are shown in Fig. 4. A relatively stable cavity covers the entire hydrofoil's suction surface, extending beyond the trailing edge; and a distinct interface forms between water and cavitating flow regions, which is called the cavity boundary. Generated from the foil's leading (the lower vortex) and the rear blunt edge (the upper vortex), the cavitation vortices shed from the cavity tail. Thus, the main characteristics of this stage can be characterized as fluctuating cavity with continuous vortex shedding.

Especially, the time-dependent numerical results show that the interface between two-phase mixture region to vapor region is always in reverse motion, which indicates the variation of the two-phase volume fraction in the cavity. Also as shown in Fig. 4, at time t1, the water-vapor interface forms at the cavity trailing (at time t1), and continues to motion adversely. At time t1+12, the interface moves adversely to the middle part of the cavity, and until to the foil suction section (at time t1+20).

Fig. 5 shows the instantaneous pressure distributions along L1, L2 and L3 inside the cavity respectively. Although the numerical values are continuous, appropriate sampling points are selected for convenient plotting. Here, the saturated vapor pressure, Psat, is 3168 Pa. It's found that substantial pressure fluctuating occurs at two positions in all the cases. Firstly, corresponding to the cavity trailing, the pressure fluctuates violently with time varies. Apparently, it indicates the pressure difference between the cavitation area and the main stream area. Secondly, at some position inside the cavity, the instantaneous pressure drops soon after increasing above Pv. And, the pressure fluctuating position moves toward the foil's suction section with time. Corresponding to the distribution of vapor volume fraction in Fig. 4, the violent pressure fluctuating is just related to the reverse motion of the water-vapor interface. That's to say, the water-vapor interface motions adversely with the change of the pressure fluctuating position.

Fig. 6 shows the two-phase velocity distributions along L1, L2 and L3 inside the cavity, respectively. Similar with the pressure distributions, two characteristics can be observed. Firstly, at the cavity trailing, the velocity fluctuates violently. Secondly, distinct difference of velocity distributions appears between the vapor region and two-phase mixture region. In the vapor region, the water velocity is close to zero, and with lower vapor velocity (about 10 percent of the main-stream one). However, higher velocity distributions are obtained in the two-phase region, and fluctuate in the range of 0~60 percent of the main-stream velocity. What's more, the higher velocity area expands adversely with the reverse motioning of two-phase region.

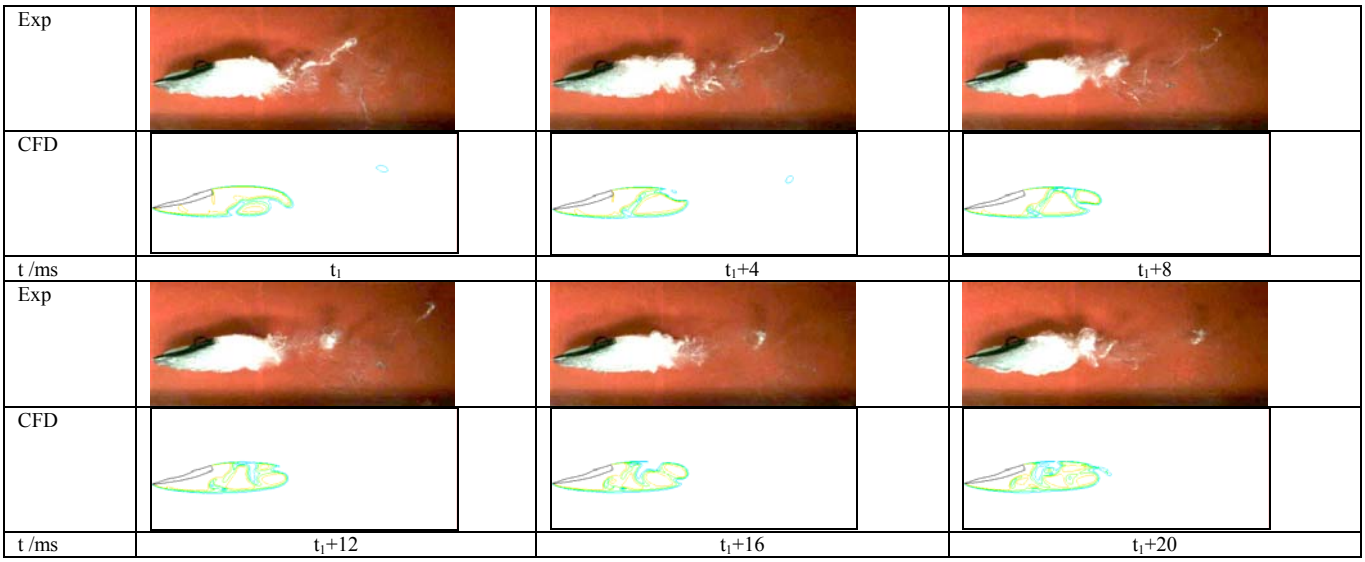

Fig. 4 CFD simulation compared with flow visualizations (σ= 0.74)

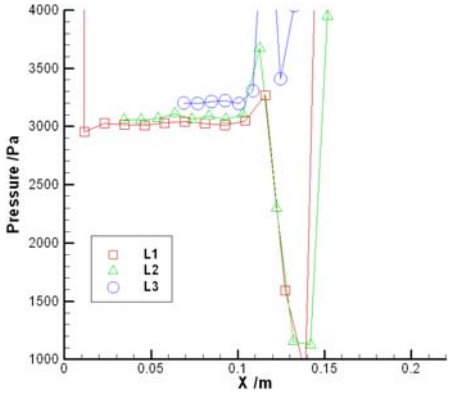	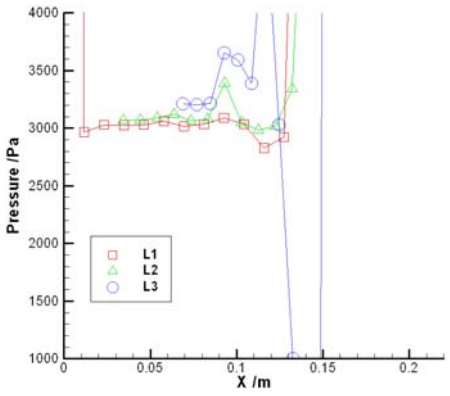
t_1+12	t_1+16
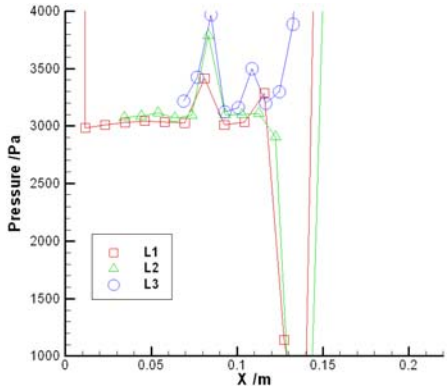	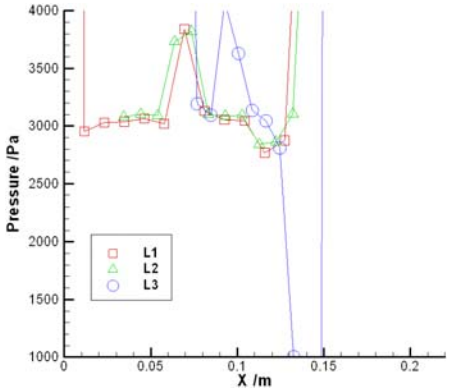
t_1+20	t_1+24

Fig. 5 Instantaneous pressure distributions inside the cavity (σ= 0.74)

time (ms)	Water-phase	Vapor-phase
t_1+12	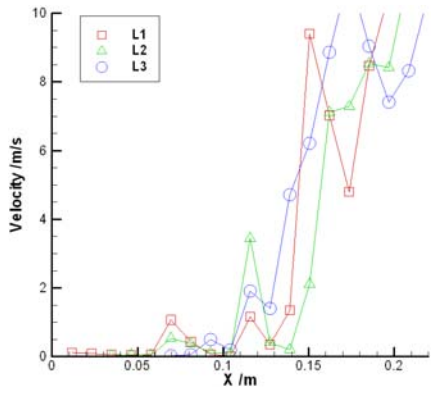	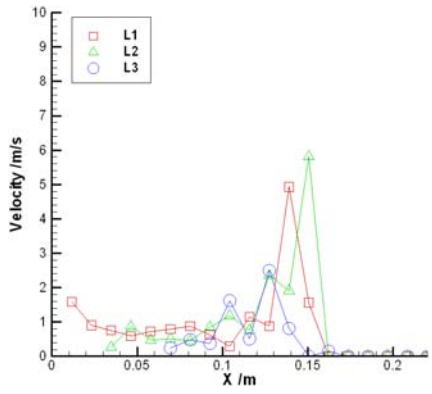

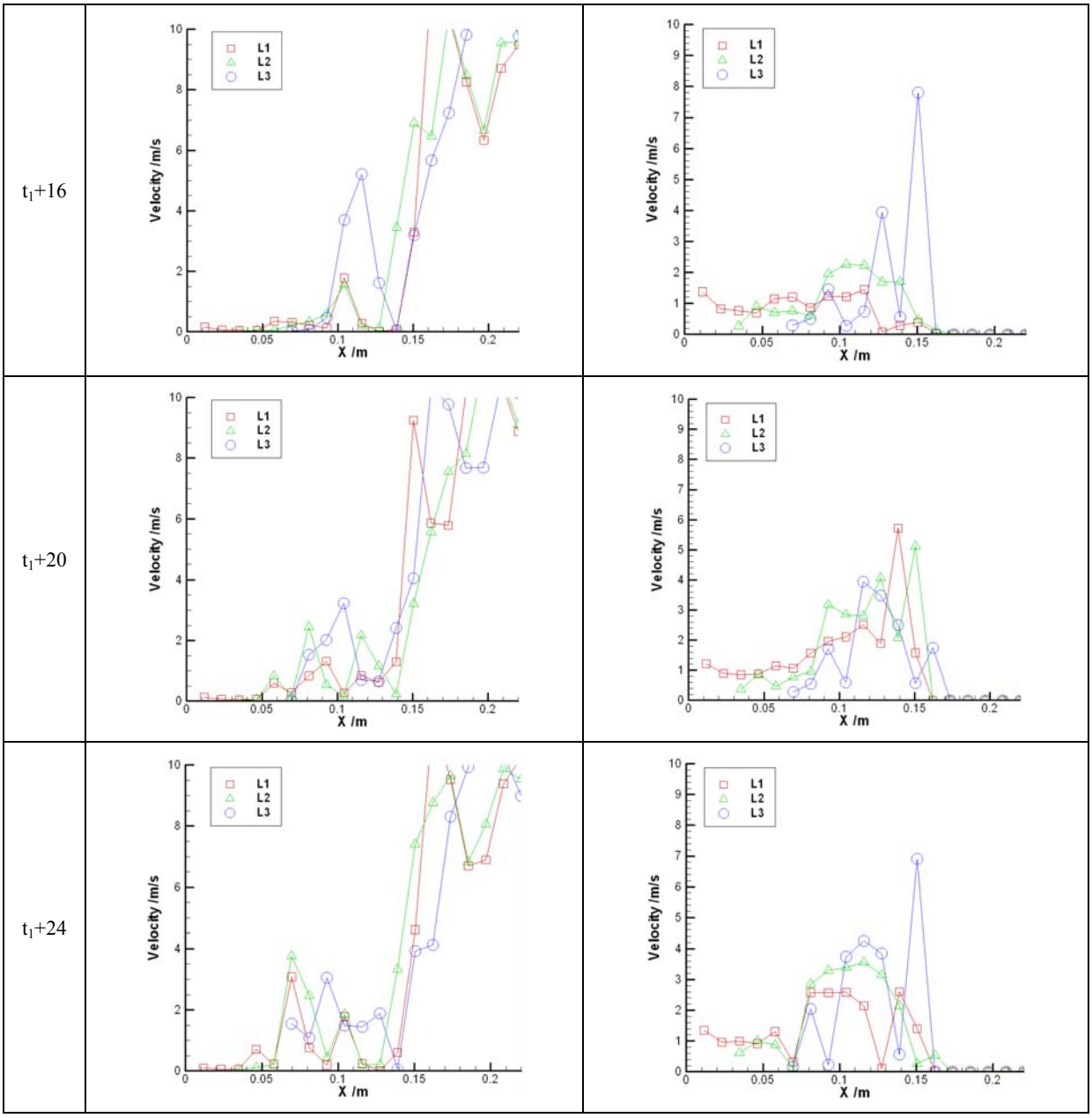

Fig. 6 Instantaneous velocity distribution inside the cavity (σ= 0.74)

Further lowering the cavitation number, the cavity becomes larger and longer. Fig. 7 shows CFD simulation compared with the flow visualizations [36], when the cavitation number is 0.54. Both of experimental and numerical results show a transparent region near the hydrofoil suction surface, which indicates that the cavity's front is largely filled with vapor, and two-phase mixture in the rear region. A distinct interface between the two zones can be seen, noted with a black line. Obviously, the interface location is highly unsteady too. A more detailed illustration of the interface movement is presented based on the numerical simulation. After the water-vapor interface forms at the cavity trailing at time t1, it continues to motion adversely, and moves to the same location with the experimental one at time t1+60, until to the foil suction section at time t1+80.

Fig. 8 shows the instantaneous pressure distribution inside the cavity as σ= 0.54. Similar characteristics can be obtained as σ= 0.74. It shows that at this condition, while the pressure in the pure vapor region is essentially the same as the vapor pressure, and the averaged pressure in the mixture region can be somewhat higher, the hydrodynamics and associated momentum transfer can create further pressure difference

between these two zones to induce time dependency of the interface location. Under supercavitation condition, even though the cavity boundary seems to be quite steady, the pressure fluctuation and unsteady mass transfer process can still be substantial inside the cavity, between the vapor and the two-phase regions. Fig. 9 shows the instantaneous velocity distribution correspondingly. Compared with Fig. 6, the same characteristics of velocity fluctuation can be observed, but the velocity fluctuating range when the cavitation number is 0.54 becomes smaller than that at σ= 0.74.

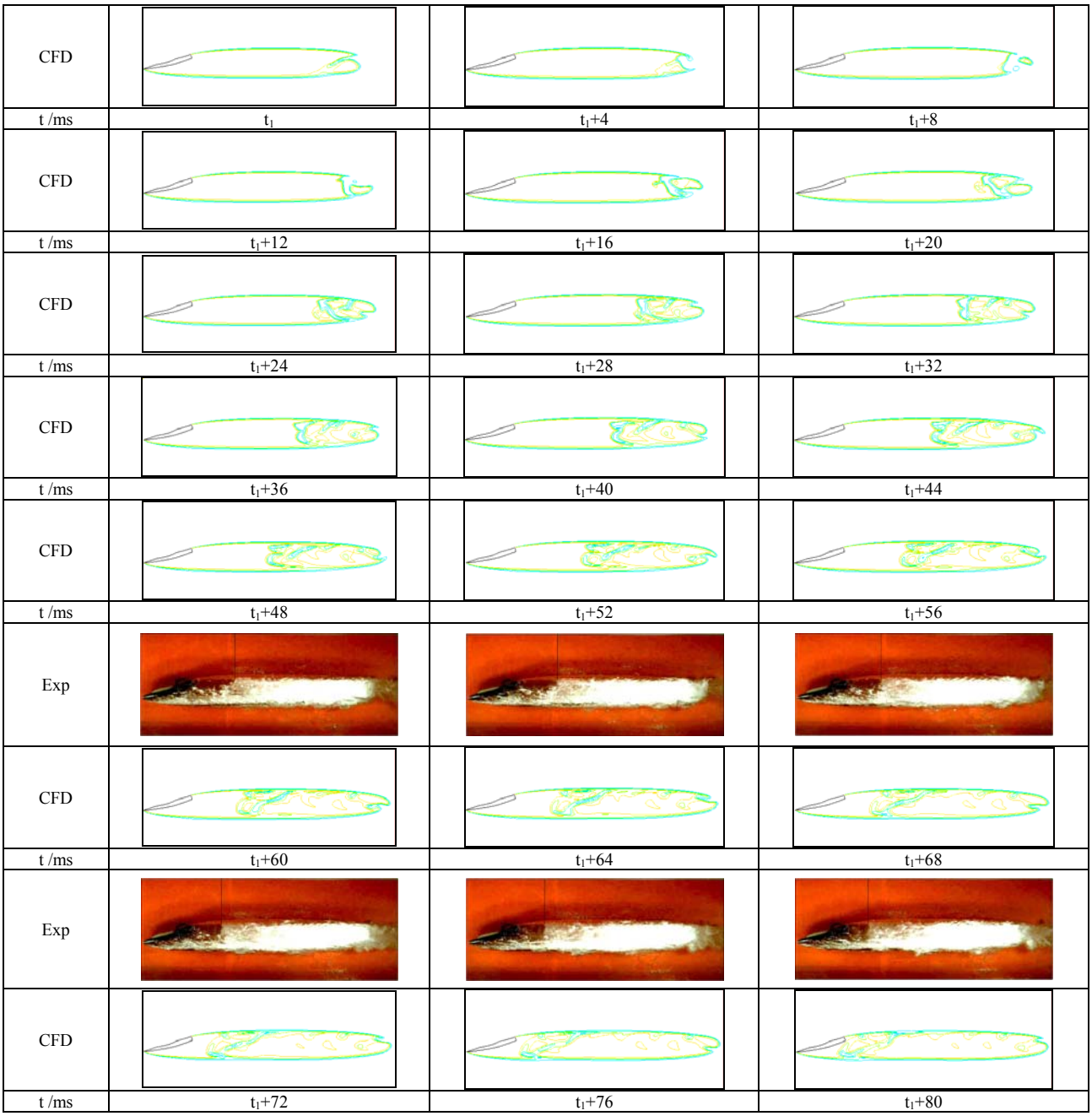

Fig. 7 Flow visualization of experiment and CFD simulation (σ= 0.54)

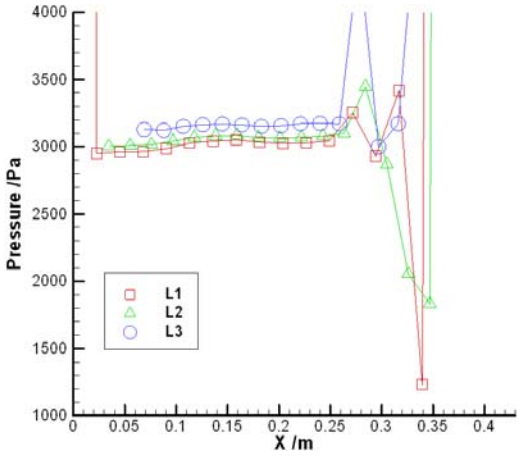

t_1+12

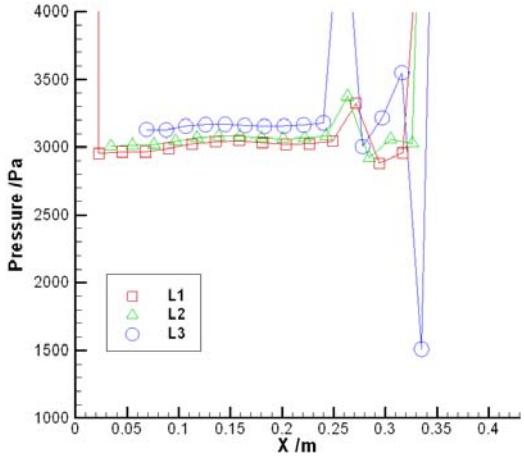

t_1+16

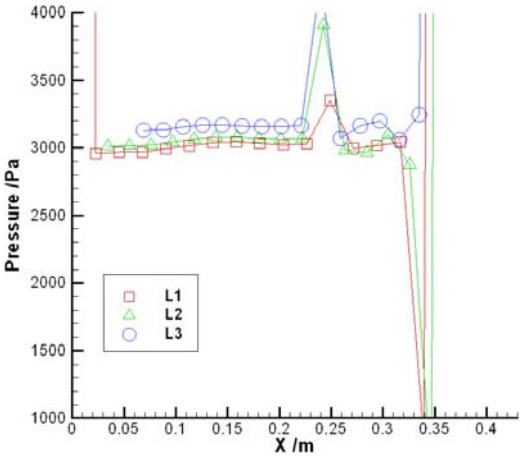

t_1+20

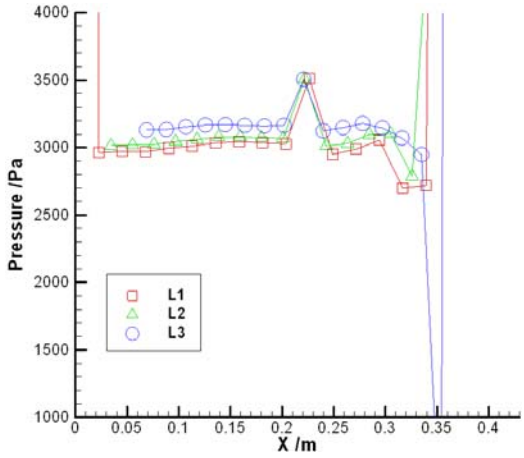

t_1+24

Fig. 8 Instantaneous pressure distribution inside the cavity (σ= 0.54)

time (ms)	Water-phase	Vapor-phase
t_1+12	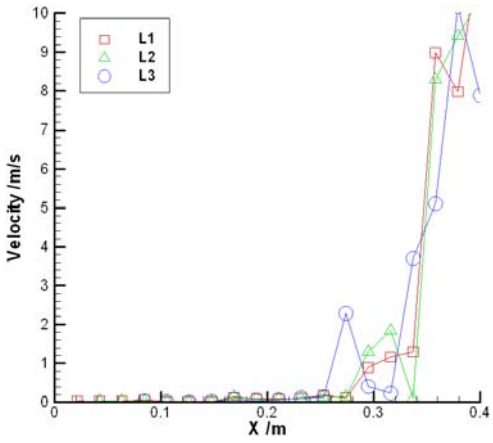	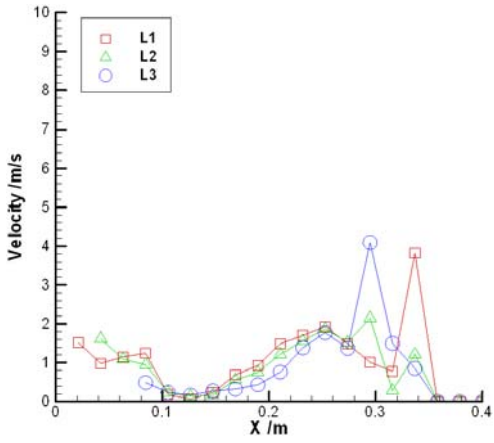

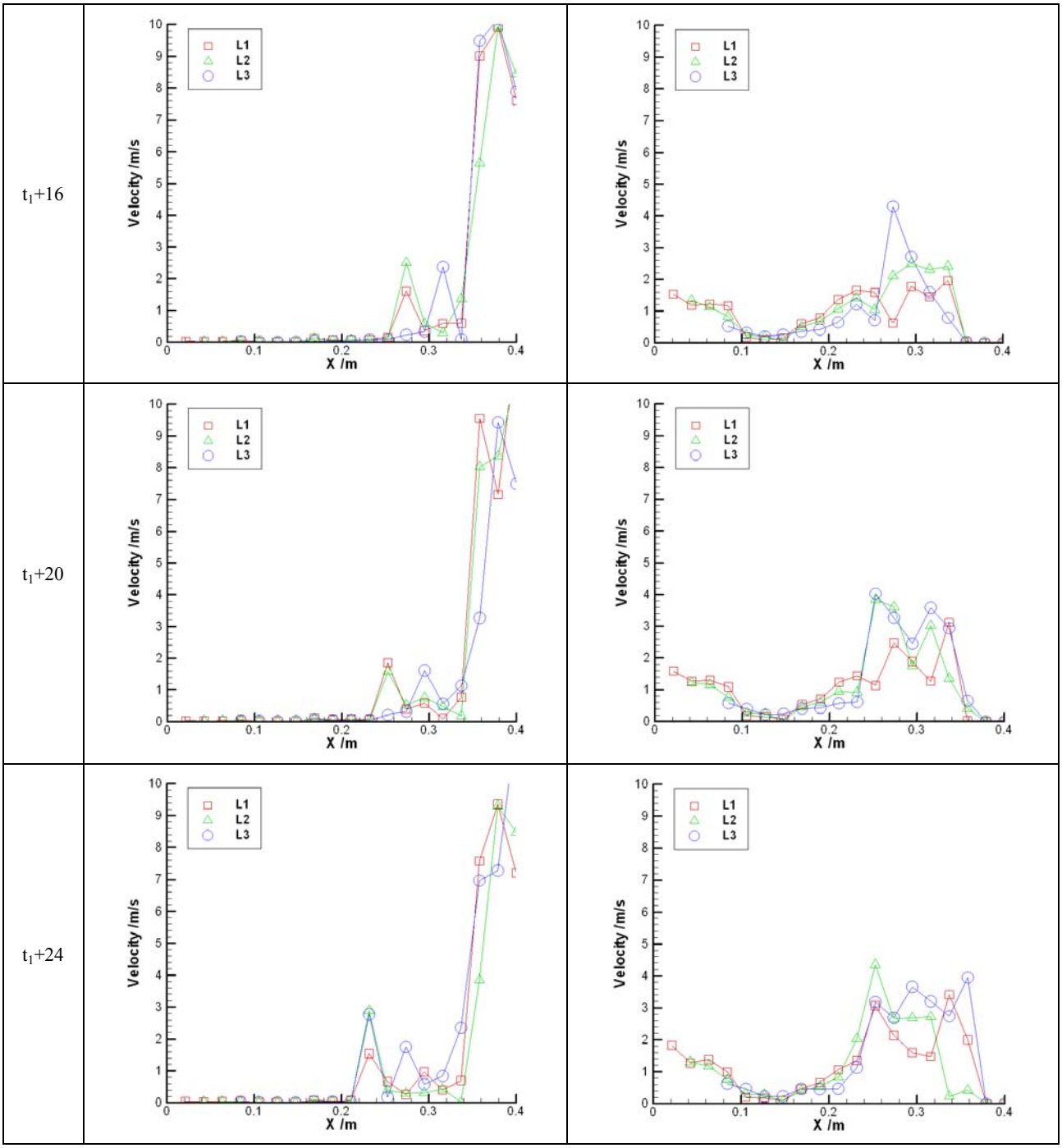

Fig. 9 Instantaneous velocity distribution inside the cavity (σ= 0.54)

3. CONCLUSION

The supercavitating flow around a hydrofoil is investigated numerically. The modified RNG k-ε turbulence model is imposed in the numerical simulation. The computational results are compared with experimental ones. It's found that the numerical results agree well basically with the experimental one in the flowing structures. It is clearly shown that the cavitation structure depends on the interaction of the water-

vapor mixture and the vapor among the whole cavitation stage. The interface between the vapor and the two-phase mixture exhibits substantial unsteadiness, indicating frequent mass transfer processes occurring inside the cavity.

The adverse motion of the two-phase interface relates to the pressure and velocity variation inside the cavity. Corresponding to the interface position, violent pressure and velocity fluctuating occurs, and the fluctuating section moves adversely with time varies. And, the velocity in the vapor region is lower than that in the two-phase region.

NOMENCLATURE

C	chord length of hydrofoil
$C_{\varepsilon 1RNG}, C_{\varepsilon 2RNG}, C_{\mu RNG}$	empirical constants
F_e, F_c, α_{nuc}	empirical constants
K	turbulent kinetic energy
$\dot{m}^+$	evaporation rate
$\dot{m}^-$	condensation rate
n	empirical constant
P_B	pressure in the vapor bubble
P_{sat}	saturated vapor pressure
P_{turb}	local turbulent pressure fluctuating
P_v	phase-change threshold pressure of vapor
P_∞	reference static pressure
R_B	vapor bubble radius.
Re	Reynolds number
S	bubble surface tension
U	reference velocity
U	velocity component in x-direction
V	velocity component in y-direction
α_v	vapor volume fraction
ε	turbulent dissipation rate
μ	liminar viscosity
μ_t	turbulent viscosity
ν	kinematic viscosity
ρ	density of liquid-vapor mixture
ρl	density of liquid
ρv	density of vapor
σ	cavitation number
$\sigma_{kRNG}, \sigma_{\varepsilon RNG}$	empirical constant

ACKNOWLEDGMENTS

The authors gratefully acknowledge support by the National Natural Science Foundation of China (NSFC, Grant No.: 50679001).

REFERENCES

[1] Wang G.Y., Senocak I., Shyy W., Ikohagi T., Cao S.L.: Dynamics of attached turbulent cavitating flows. Prog Aerosp Sci 37, 551–581, 2001

[2] Brennen C.E.: Cavitation and bubble dynamics. New York: Oxford University Press, 1995

[3] Rood E.P.: Review-mechanisms of cavitation inception. J Fluids Eng 113, 163-175, 1991

[4] Kawanami Y., Kato H., Yamauchi H., Tanimura M., Tagaya Y.: Mechanism and control of cloud cavitation. J Fluids Eng 119, 788-794, 1997

[5] Leger A.T. and Ceccio S.L.: Examination of the flow near the leading edge of attached cavitation. Part1. detachment of two-dimensional and axisymmetric cavities. J Fluid Mech 376, 61-90, 1998

[6] Delange D.F., Debruin G.J.: Sheet cavitation and cloud cavitation, re-entrant jet and three-dimensionality. Appl Sci Res 58, 91–114, 1998

[7] Kjeldsen M., Arndt R.E.A., Effertz M.: Spectral characteristics of sheet/cloud cavitation. Transactions of the ASME, J Fluids Eng 122, 481-487, 2000

[8] Hrubes J.D.: High-speed imaging of supercavitating underwater projectiles. Exp in Fluids 30, 57-64, 2001

[9] Shen and Dimotakis: The influence of surface cavitation on hydrodynamic forces. in Proceedings 22nd ATTC. St. Johns, 1989

[10]Wu Y.T. and Wang D.P.: A wake model for free-streamline flow theory, part 2. cavitating flows past obstacles of arbitrary profile. J Fluid Mech 18, 65-93, 1963

[11]Furness R.A., Hutton S.P.: Experimental and theoretical studies of two-dimensional fixed-type cavities. J Fluids Eng 97, 515-522, 1975

[12]Lee C.S., Kim Y.G., Lee J.T.: A potential–based panel method for the analysis of two-dimensional super- or partially-cavitating hydrofoils. J Ship Res 195, 168-181, 1992

[13]Chen Y. and Heister S.D.: A numerical treatment for attached cavitation. J Fluids Eng 116, 613-618, 1994

[14]Wu J. Y., Wang G. Y., Shyy W.: Time-dependent turbulent cavitating flow computations with interfacial transport and filter-based models. Int J Numer Meth In Fluids 49, 739-761, 2005

[15]Delannoy Y., Kueny J.L.: Two phase flow approach in unsteady cavitation modelling. ASME Fluids Eng Div Publ FED 98, 153-158,1990

[16]Gopalan S. and Katz J.: Flow structure and modeling issues in the closure region of attached cavitation. Phys Fluids 12, 895-911, 2000

[17]Senocak I., Shyy W.: Evaluation of cavitation models for Navier-Stokes computations. ASME Fluids Eng Div Publ FED 257, 395-401, 2002

[18]Senocak I., Shyy W.: Interfacial dynamics-based modelling of turbulent cavitating flows, Part-1: model development and steady-state computations. Int J Numer Methods Fluids 44, 975-995, 2004

[19]Singhal A.K., Vaidya N., Leonard A.D.: Multi-dimensional simulation of cavitating flows using a PDF model for phase change. ASME Fluids Eng Div Publ FED 4, 7p, 1997

[20]Kunz R.F., Boger D.A., Stinbring D.R.: A preconditioned navier-stokes method for two-phase flows with application to cavitation prediction. Comput Fluids 29, 849-875, 2000

[21]Senocak I., Shyy W.: A pressure-based method for turbulent cavitating flow computations. J Comput Phys 176, 363-383, 2002

[22]Senocak I., Shyy W.: Interfacial dynamics-based modelling of turbulent cavitating flows, Part-2: Time-dependent computations. Int J Numer Methods Fluids 44, 997-1016, 2004

[23]Singhal A.K., Athavale M.M., Li H.Y., Jiang Y.: Mathematical basis and validation of the full cavitation model. J Fluids Eng 124, 617-624, 2002

[24]Wu J., Utturkar Y., Senocak I.: Impact of turbulence and compressibility modeling on three-dimensional cavitating flow computations. AIAA, 2003

[25]Shyy W.: A study of finite difference approximations to steady-state, convection-dominated flow problems. J Comput Phys 57, 415-438, 1985

[26]Shyy W.: A numerical study of annular dump diffuser flows. Comput Methods Appl Mech Eng 53, 47-65, 1985

[27]Vaidyanathan, R., Senocak I., Wu J. and Shyy W.: Sensitivity evaluation of a transport-based turbulent cavitation model. J Fluids Eng 125, 447-458, 2003

[28]Coutier-delgosha O., Fertes-Patella R., Reboud J.L.: Evaluation of the turbulence model influence on the numerical simulation of unsteady cavitation. J Fluids Eng Trans ASME 125, 38-45, 2003

[29]Yuan W., Schnerr G.H., Optimization of two-phase flow in injection nozzles-interaction of cavitation and external jet formation, Proc. of ASME fluids engineering, Summer meeting, 2002.

[30]Yakhot V., Orszag S.A., Renormalization group analysis of turbulence: I. basic theory, J Sci Comput, (1)1-51, 1986

[31]Yakhot V., Orszag S.A., Thangam S., Gatski T.B., Speziale C.G.: Development of turbulence models for shear flows by a double expansion technique. Phys Fluids A, Fluid Dyn 4, 1510-1520, 1992

[32]Johansen S. T., Wu J.Y., Shyy W.: Filter-based unsteady RANS computations. Int J Heat Fluid Flow 25, 10-21, 2004

[33]Kubota A., Kato H., Yamaguchi H.: A new modelling of cavitating flows: a numerical study of unsteady cavitation on a hydrofoil section. J Fluid Mech 240, 59-96, 1992

[34]Keller A.P., Rott H.K.: Effect of flow turbulence on cavitation inception. ASME Fluids Eng Div Publ FED 4, 3p, 1997

[35]Stoffel B., Schuller W.: Investigations concerning the influence of pressure distribution and cavity length on hydrodynamic cavitation intensity. ASME Fluids Eng Div Publ FED 226, 51-58,1995

[36]Wang G., Li X., Zhang M., Shyy W., Multiphase dynamics of supercavitating flows around a hydrofoil, *Sixth International Symposium on Cavitation, CAV2006,* Wageningen, The Netherlands, September